Indirect pumping bell–bloom magnetometer*

Meng-Bing Wang(王梦冰)[1], Da-Fa Zhao(赵大法)[2], Gui-Ying Zhang(张桂迎)[1,3], and Kai-Feng Zhao(赵凯锋)[1,†]

[1] *Institute of Modern Physics, Fudan University, Shanghai* 200433, *China*
[2] *Department of Nuclear Science and Technology, Fudan University, Shanghai* 200433, *China*
[3] *Department of Applied Physics, Zhejiang University of Technology, Hangzhou* 310023, *China*

(Received 10 April 2017; revised manuscript received 8 June 2017; published online 10 September 2017)

When the ground state hyperfine splitting of alkali metal vapor atoms is well optically resolved, the spin coherence on one hyperfine sublevel can be generated directly or indirectly by pumping the same or the other sublevel respectively. We experimentally studied the pump power dependence of the field response of a Bell-Bloom magnetometer for the two pumping schemes in a paraffin coated ^{87}Rb vapor cell. We find that although the maximum field response is achieved by combining the two pumping schemes, indirect pumping alone can do nearly as good while being much simpler to operate. We have achieved a sensitivity of 100 fT/Hz$^{1/2}$ with a single indirect pump at room temperature.

Keywords: indirect pumping, anti-relaxation coating, power broadening, magnetometry

PACS: 07.55.Ge, 32.80.Xx, 76.60.Es, 76.70.Hb **DOI:** 10.1088/1674-1056/26/10/100701

1. Introduction

Bell–Bloom magnetometer (BBM) is based on the principle that a large atomic ground state spin coherence can be generated by synchronous transverse pumping modulated at the frequency near the Larmor frequency of the bias magnetic field.[1] Compared to the double resonance magnetometer, BBM has its advantage of being all optical, which does not produce any radio frequency fields, and has become an important type of atomic magnetometer.[2–7] The precession of the atomic spin polarization can be monitored by the paramagnetic Faraday rotation of another linearly polarized probe beam.[8] Such geometry is back-action evading and has the potential of achieving sensitivities beyond the standard quantum limit.[9]

The sensitivity of a magnetometer is given by the ratio of the signal's noise, which is the signal fluctuation due to anything except the magnetic field, to the signal's field response, which is the slope of the change of signal with respect to the change of field. The field response is proportional to the magnitude of the spin polarization and the total relaxation time of spin coherence,[2] which is mostly determined by atom–atom spin exchange collision relaxation,[10] atom–wall collision relaxation,[11] and optical pumping power-broadening. The spin exchange relaxation could be suppressed by operating the magnetometer in the spin-exchange relaxation free (SERF) mode[12,13] or by pumping all the atoms to the stretched state.[14] Wall relaxation could be suppressed by either using cells filled with inert buffer gas[13] or cells coated by anti-relaxation coatings.[11,15] Optical pumping induces spin decoherence due to the de-population process, where the atoms are pumped out of states whose polarization is being probed.

In anti-relaxation coated cells, without pressure broadening caused by buffer gas, the ground state hyperfine structure is well resolved and the light could be resonant with the transition coupling the excited states with either the $F_a = I + S$ or the $F_b = I - S$ ground state hyperfine sublevel where F, I, and S are atomic, nuclear, and electronic spin quantum numbers respectively. Likewise, polarization on either hyperfine sublevel could be probed separately. When the polarization on one hyperfine sublevel is to be probed, it can be generated by pump light resonant either with the same or the other hyperfine sublevel, which are respectively named direct pumping (DP) and indirect pumping (IP) in this paper. For double resonance magnetometer, Julsgaard *et al.*[16] found that indirect pumping along the magnetic field direction does not cause any power-broadening of magnetic resonance linewidth. Chalupczak *et al.*[17,18] found that the efficiency of indirect pumping could be enhanced by spin exchange collisions, which results in a narrowing of resonance line shape due to high population occupation of the stretched spin state. For BBM, the effect of indirect pumping on the amplitude and linewidth of Cesium magnetic resonance was studied for different angles between the bias magnetic field and the propagation direction of the pump beam.[19] Here we compared direct, indirect and combined pumping schemes for an ^{87}Rb BBM operating at room temperature. The best sensitivity achieved by a single indirect pump beam is 100 fT/Hz$^{1/2}$. We also found amplitude reduction and line broadening effects of indirect pumping at higher pump powers.

*Project supported by the Natural Science Foundation of Shanghai (Grant No. 16ZR1402700), the National Natural Science Foundation of China (Grant No. 91636102), and the National Key Research and Development Program of China (Grant No. 2016YFA0302000).

†Corresponding author. E-mail: zhaokf@fudan.edu.cn

© 2017 Chinese Physical Society and IOP Publishing Ltd

2. Theoretical method

Our experiment is modeled by the following simplified theory. We assume that the bias magnetic field is along the $\hat{y}$ axis, the circular polarized pump light propagates along the $\hat{z}$ axis, and the linearly polarized probe light propagates along the $\hat{x}$ axis with polarization along $\hat{y}$ axis, as shown in Fig. 1.

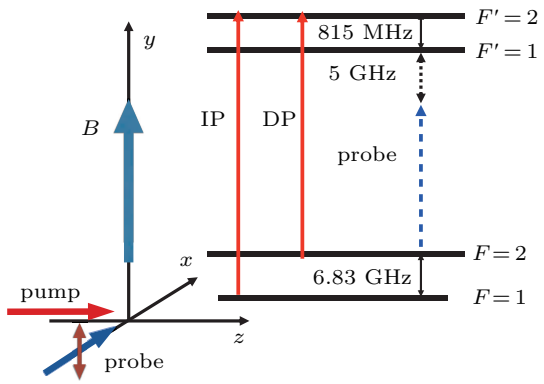


Fig. 1. (color online) Schematic diagram of the BBM: energy structure of the ^{87}Rb $5^2S_{1/2} \longrightarrow 5^2P_{1/2}$ transition (D_1 line, 795 nm). DP: direct pump light resonant with ground state $F = 2$ to excited state $F' = 2$. IP: indirect pump light resonant with the ground state $F = 1$ to excited state $F' = 2$. The probe light detects the polarization on $F = 2$ hyperfine state with frequency red detuned 5 GHz away from the $F = 2$ to $F' = 1$ transition. Both pumps are circularly polarized and the probe is linearly polarized.

The time evolution of ground state density matrix $\hat{\rho}$ is given by[20]

$$i\hbar\frac{d}{dt}\hat{\rho} = [\hat{H},\hat{\rho}] - \frac{1}{2}i\hbar(\hat{\Gamma}\hat{\rho} + \hat{\rho}\hat{\Gamma}) + i\hbar\hat{\Lambda}, \tag{1}$$

where $\hbar$ is the Planck constant. We define $[F_a] \equiv 2F_a + 1$ and $[F_b] \equiv 2F_b + 1$ as the number of Zeeman sublevels in the F_a and F_b hyperfine sublevels respectively. The density matrix has a dimension of $[F_a] + [F_b]$ with indices ranging over all the Zeeman levels of the ground state.

The Hamiltonian $\hat{H}$ represents the interaction between atoms and the magnetic field, and is given by

$$\hat{H} = -\hat{\mu}_y B = \gamma B\hat{F}_y = 2\pi\nu_0\hat{F}_y, \tag{2}$$

where ν_0 is Larmor frequency of atom in the magnetic field of strength B.

The depopulation matrix $\hat{\Gamma}$ is a diagonal matrix with elements representing the population loss of the i-th Zeeman level

$$\Gamma_{ii}(t) = \Gamma_0 + c_i R(t), \tag{3}$$

where Γ_0 is the isotropic depopulation dark-relaxation rate common to all the Zeeman levels and $R(t)$ is the depopulation pumping rate. The coefficient c_i is the relative line strength of the i-th Zeeman level exited by the pump light, and is zero for unpumped Zeeman levels. The conservation of probability requires $\sum_i c_i = 1$.

The repopulation matrix $\hat{\Lambda}$ is also diagonal with elements representing the population gain of the i-th Zeeman level

$$\Lambda_{ii}(t) = \sum_j f_{ij}c_j R(t)\rho_{jj} + \frac{\Gamma_0}{[F_b] + [F_a] - 1}\sum_{k\neq i}\rho_{kk}. \tag{4}$$

The first term on the right-hand side describes the population gain due to pumping. And the summation over j includes only the pumped Zeeman levels. The coefficient f_{ij} denotes the branching ratio of atoms transferred from the j-th Zeeman level to the i-th one through depopulation pumping and spontaneous de-excitation. And the conservation of probability requires $\sum_i f_{ij} = 1$. The second term describes the population gain due to dark relaxation. And the summation over k includes all ground state Zeeman levels except the i-th one. We assume that the dark-relaxation rates are the same for all Zeeman levels and the population loss from one Zeeman level is distributed equally to all other $[F_b] + [F_a] - 1$ Zeeman levels. By doing so, we have greatly simplified the complex roles of wall relaxation and spin exchange relaxation, it should be valid if they are both very small, which is met by our experimental condition with high quality antirelaxation coated vapor cells running at low vapor density. Finally, The probe light detects the orientation of the upper hyperfine state along the $\hat{x}$ axis, $\langle\hat{F}_{ax}\rangle$, which is given by

$$\langle\hat{F}_{ax}\rangle = \mathrm{tr}(\rho\hat{F}_{ax}). \tag{5}$$

To simulate the operation of a BBM, we assume $R(t)$ is a sinusoidal function of the form $R(t) = R_0[1 + \cos(2\pi\nu t)]$ with $\nu, \nu_0 \gg \Gamma_0, R_0$. Although in the actual experiment we use a square wave polarization modulation, the final result should not have any qualitative difference.[20] The numerical solution of $\langle F_{ax}(t)\rangle$ for $t \gg 1/(\Gamma_0 + R_0)$ evolves into a steady state oscillation with frequency ν and amplitude $F_\infty(\Delta\nu)$, which is a Lorentzian like function with respect to the detuning $\Delta\nu = \nu - \nu_0$.

The calculated pumping rate dependence of the peak value and linewidth (full width half maximum) of F_∞ are plotted in Fig. 2 and Fig. 3 respectively. In the calculation, we set all other rates and frequencies in unit of the dark-relaxation rate.

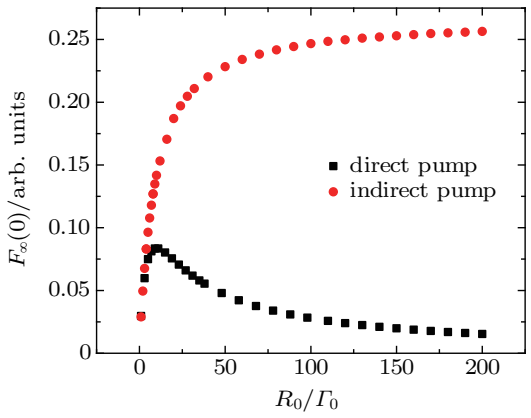


Fig. 2. (color online) Calculated results of the dependence of the steady state orientation amplitude on the direct (black square) and indirect (red circle) pumping rate.

Figure 2 shows the pumping rate dependence of $F_\infty(\Delta\nu)$'s peak value $F_\infty(0)$. For the case of direct pumping, $F_\infty(0)$ first increases and then decreases with the pumping rate. This is due to the competition between the increase of polarization versus the decrease of population on F_a. For indirect pumping, $F_\infty(0)$ keeps increasing with pump power, and eventually saturates for high pumping rates.

Figure 3 shows the pumping rate dependence of the linewidth of $F_\infty(\Delta\nu)$. For direct pumping, the linewidth increases linearly with the pumping rate. For indirect pumping, the linewidth is independent of the pumping rate.

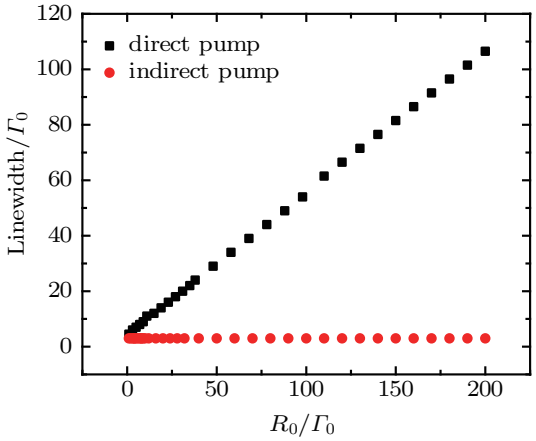


Fig. 3. (color online) Calculated results of the dependence of the linewidth of Lorentzian function $F_\infty(\Delta\nu)$ on the direct (black square) and indirect(red circle) pumping rate.

By comparing the pump rate dependence of the amplitude and linewidth between the direct and indirect pumping scheme, one can see that indirect pumping can give a large amplitude free from power-broadening. There is a possibility that the magnetometry with higher sensitivity can be achieved.

3. Experimental setup

The schematic design of the experiment is shown in Fig. 4. The experiment was performed on isotopically enriched Rb (99.5% ^{87}Rb) vapor atoms contained in a cubic borosilicate glass cell (size 20 mm × 20 mm × 20 mm) with no buffer gas. To reduce the wall relaxation of spin coherence, the inner surface of the cell was coated with Tetratetracotane according the method described by Seltzer, Bouchiat, and Balabas.[22] The cell is mounted inside a 4-layer cylindrical μ-metal shield and is kept at room temperature, corresponding to a rubidium density of about 5×10^9 cm^{-3}. A coil system provides a uniform magnetic field within the volume of the cell. The strength of the field corresponds to a Larmor frequency of 17 kHz for the ground state of ^{87}Rb. Two 795 nm distributed feed-back (DFB) lasers (UniQuanta) individually resonant with the $F=2\rightarrow F'=2$ and $F=1\rightarrow F'=2$ transitions act as the direct and the indirect pump respectively. The two beams are combined into a single one, whose polarization is square-wave modulated between the σ^+ and the σ^- states by an electro-optical modulator (EOM). Finally the pump beam is expanded to 2 cm in diameter before entering the cell. The probe beam is provided by an 795-nm external-cavity-diode-laser (Toptica DLpro) whose frequency is red-detuned about 5 GHz from the $F=2$ to $F'=1$ transition in order to render negligible absorption. The probe beam is linearly polarized, and has a diameter of 4 mm and power of 0.4 mW. The paramagnetic Faraday rotation (PFR) of the probe is measured by a balanced polarimeter connected to a lock-in amplifier (SRS SR830) referenced to the modulation frequency of the pump. The lock-in's time constant is set at 1 ms and roll off 24 dB/oct corresponding to an equivalent noise bandwidth of 78 Hz. When the polarization modulation frequency of the pump is scanned through the Larmor frequency of the field, a dispersive magnetic resonance signal can be obtained from the quadrature output of the lock-in.

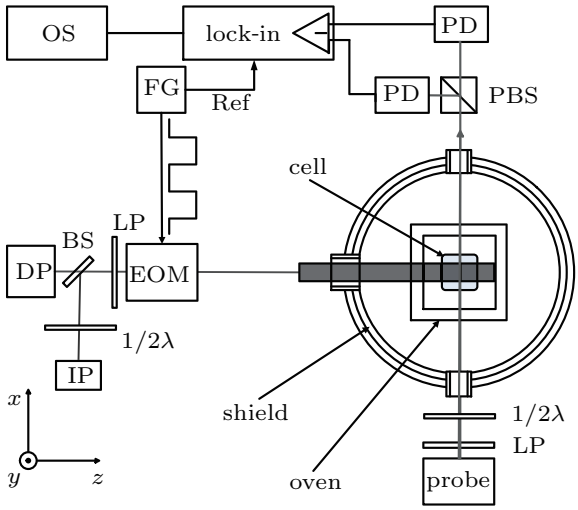


Fig. 4. Direct and indirect pumping light are combined in BS and modulated by EOM and then enter the cell. The linear polarized probe light is detuned to the red and the rotation angle is monitored by the balanced detector by the Lock-in. The modulation signal and its reference signal is send to the EOM and Lock-in respectively. DP, IP: the direct and indirect pumping light. FG: frequency generator.

4. Results and discussion

Figure 5 shows a typical dispersive Lorentzian signal recorded by the lock-in amplifier for indirect pumping. The pump power is 0.24 μW and is square-wave modulated between $\sigma+$ and $\sigma-$ polarized light. The cells temperature is 25.4 °C. The horizonal difference between the two peaks is the signal linewidth and vertical difference the signal amplitude. The absolute value of the slope at the resonance center represents the field response of the magnetometer.

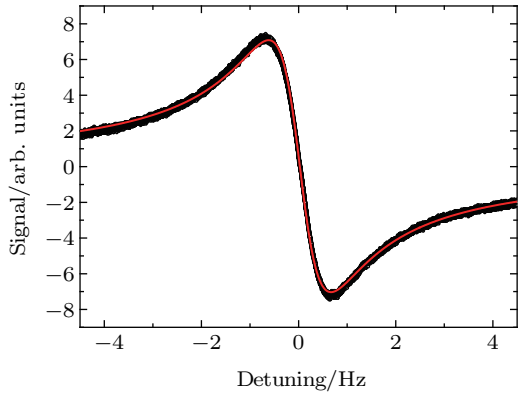


Fig. 5. (color online) The experimental dispersive Lorentzian signal obtained from the Lockin amplifier by scanning the modulation frequency ν across the Larmor frequency. The cell temperature is 25.4 °C. The red line is the Lorentzian fit corresponding to the linewidth of 1.3 Hz.

4.1. Comparison of direct pumping and indirect pumping

In this section, we compared the pump power dependence of the amplitude and linewidth for direct and indirect pumping schemes. Figure 6 shows the dependence of amplitude on the pump light power for both the direct and the indirect pumping schemes. For light power less than 4 μW, the amplitude in both case increases at nearly the same rate. For pump light power larger than 4 μW, the amplitude of direct pumping scheme dramatically decreases,This is the result of a large population of atoms being pumped from the $F = 2$ to the $F = 1$ hyperfine sublevel, despite of high orientation on the $F = 2$ sublevel. The amplitude of indirect pumping continue to increase and reaches its maximum at about 20 μW and then start to decrease. In a previous study on Cesium,[19] the signal amplitude continuous to increase with the indirect pumping power. However, they used a closed transition of D2 line for pumping, while here an open transition of D1 line is used. Figure 7 shows pumping power dependence of the linewidth for the two pumping schemes. When light power is increased from 0.2 μW to 40 μW, the increase of power broadening is about 30 Hz for the direct pumping, but less than 1 Hz for the indirect pumping. The slope of power broadening for direct pumping is 74 times larger than that for indirect pumping. Larger amplitude and smaller linewidth could potentially enable a more sensitive detection of magnetic field for the indirect pumping scheme.

The experimental results shown in Figs. 6 and 7 are very similar to the numerical simulations shown in Figs. 2 and 3. However, there are two noticeable discrepancies for the case of indirect pumping. One is that unlike the simulation in Fig. 3 where the amplitude keeps increasing and eventually flattens at high indirect pumping rate, the experiment result in Fig. 6 shows that the amplitude will start to decrease when the indirect pumping power passes beyond certain value, and continues to decrease with increasing indirect pumping power. Another discrepancy is that unlike the simulation in Fig. 3 where there is no power broadening for indirect pumping at all, the experiment result in Fig. 7 shows a small power broadening of indirect pumping, although it is not obvious due the scale setting of that plot. In actual experiment, we increased the indirect pumping power up to 8000 μW, the linewidth will keep increasing and level off at about 20 Hz. Such a large amplitude reducing and line broadening effect was not found in the previous work on Cesium,[19] where a D_2 line closed transition was used for indirect pumping. In that work, the line broadening caused by indirect pumping is attributed to the increase of spin exchange decoherence rate due to the decrease of population imbalance caused by indirect pumping. However, in our experiment, the total dark relaxation rate contribution to the linewidth is less than 1.5 Hz, and cannot account for the large line broadening under strong indirect pumping. The amplitude reducing and line broadening effect of indirect pumping at higher pumping rate is another interesting topic. However, in this paper, since we are more concerned with the performance of magnetometer, we restrict our study in the low pumping rate region, where the signal has both large amplitude and narrow linewidth.

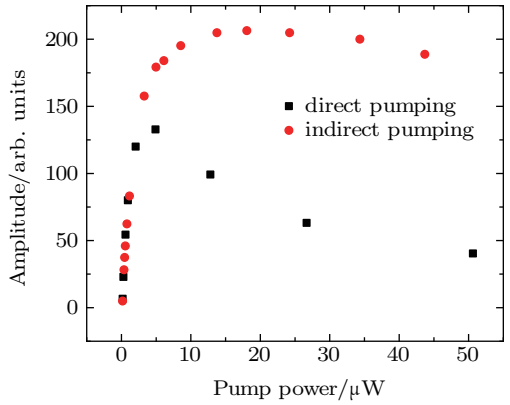


Fig. 6. (color online) The power dependence of signal amplitude for direct (black square) and indirect pumping (red circle) at 25.6 °C.

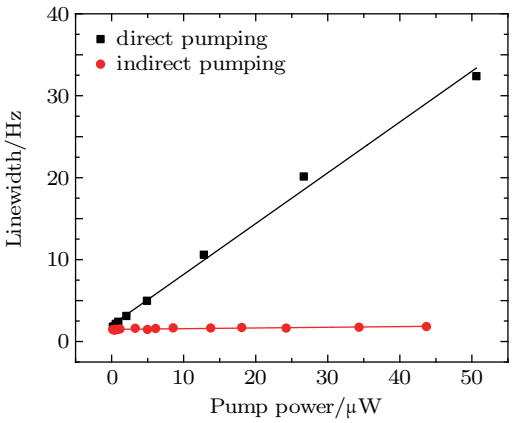


Fig. 7. (color online) The power dependence of linewidth for direct (black square) and indirect pumping (red circle) at 25.6 °C.

4.2. Field response study

The results shown in Figs. 2 and 3 indicate that indirect pumping alone will yield much larger magnetic field response than direct pumping alone. How much further improvement of field response one can obtain by combining direct and indirect pumping? To measure the field response accurately, we sinusoidally scanned the EOM's modulation frequency with an amplitude of 0.1 Hz near the center of magnetic resonance, which is equivalent to a 14-pT amplitude modulation of the bias magnetic field. The period of the frequency scan is more than 2 s, slow enough for the magnetometer to reach its steady state. As a result, the lock-in amplifier yields an oscillation signal with an amplitude proportional to the field response of the magnetometer. Figure 8 shows this field response amplitude for some representative combinations of direct and indirect pumping powers. The overall maximum value is found to be 35 a.u./pT when a 0.3-μW direct pump is combined with a 20-μW indirect pump. However, with indirect pumping alone, the maximum field response can already reach 30 a.u./pT at 19 μW, nearly as good as the best of combined pumping. Therefore, for cost-benefit and complexity considerations, optical pumping using a single indirect pump is probably a better choice in real applications.

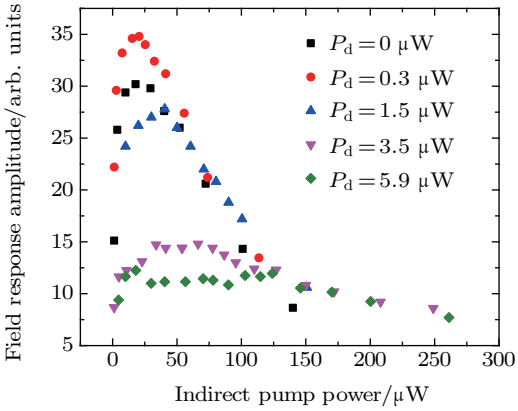


Fig. 8. (color online) The field response amplitude for different combinations of direct and indirect pumping powers. The cell temperature is 21 °C. P_d: power of the direct pump.

4.3. Sensitivity with a single indirect pump

Since we have confirmed that our pump lasers are stable enough for making little contribution to the noise of the BBM,[5] the best sensitivity of the indirect pumping scheme is achieved at the condition of maximum field response. To calibrate the signal height with the actual magnetic field, we sinusoidally scanned the EOM's modulation frequency with an amplitude of 0.01 Hz, which is equivalent to a 1.4-pT modulation of the bias field. We then record the data of signal from the lock-in amplifier for 10 s, and perform a fast Fourier transform analysis on the time series to calculate its power spectrum density.

Figure 9 shows the power spectrum density (square rooted) of the BBM with calibration signals. The relative peak height of the calibration signal decreases from 15 at 5 Hz to 8 at 40 Hz. For the calibration signal below 10 Hz, the signal's amplitude continuous to increase while the SNR remains constant, this indicates that the noise level below 10 Hz is dominated by the field fluctuations. The bandwidth of the magnetometer can be estimated to be about 7 Hz. This bandwidth could be greatly increased by self-oscillation method.[6] And the sensitivity near the bandwidth frequency is found to be 100 fT/Hz$^{1/2}$.

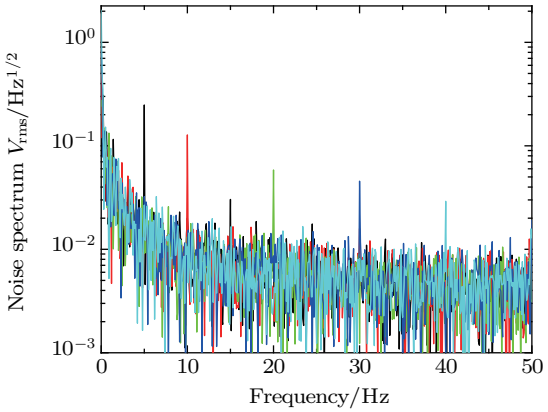


Fig. 9. (color online) Power density spectrum (square rooted) of the magnetometer. There are total 5 spectra. Each is taken with a different frequency modulation rate of the calibration signal: 5 (black), 10 (red), 20 (green), 30 (dark blue), 40 (light blue) Hz. The signal to noise ratio for each calibration signal is 14.9, 14.5, 11.0, 10.4, and 8.3 respectively. The equivalent field amplitude for the calibration signal is 1.4 pT. We plot the frequency spectrum up to 50 Hz, since the equivalent noise bandwidth of lock-in amplifier is 78 Hz.

To focus on the effect of indirect pumping on the polarization of $F = 2$ state, we have used a large detuning for the probe light to avoid detecting any polarization on the $F = 1$ state. And to avoid interference of spin exchange broadening with power broadening, the cell has been kept at room temperature where spin exchange relaxation rate is even smaller than the wall relaxation rate. These limitations can be lifted once the role of indirect pumping is understood. Therefore, the intrinsic sensitivity of indirect pumping BBM has a big room for improvement by reducing the detuning of the probe and increasing the atomic number density.

5. Conclusion

In summary, we have experimentally studied the effect of indirect pumping on an ^{87}Rb Bell–Bloom magnetometer base on high quality anti-relaxation coated cells. Such pumping scheme generates sufficient polarization with little power-broadening, and thus yields a large field response. We have also shown that adding another weak direct pump light does not make significant improvement. We have obtained a sensi-

tivity of 100 fT/Hz$^{1/2}$ in a 2-cm sized cell at room temperature. Running a magnetometer at room temperature will benefit many applications such as magnetocardiography[23] by allowing the magnetic sensor to get closer to the object. The current sensitivity is expected to have big improvement by optimizing the probe beam detuning and the atomic vapor density. Finally, we also discovered that the line broadening at high indirect pumping power exceeds what can be accounted for by other dark-relaxation rates directly, which does not agree with our simplified theoretical model as well as a previous study on Cesium atom.[19] The cause of this power broadening will be studied in the future.

References

[1] Bell W E and Bloom A L 1961 *Phys. Rev. Lett.* **6** 280
[2] Budker D, Hollberg L, Kimball D F, Kitching J, Pustelny S and Yashchuk V V 2005 *Phys. Rev. A* **71** 012903
[3] Budker D D and Romalis M 2007 *Nat. Phys.* **3** 227
[4] Pustelny S, Gawlik W, Rochester S, Kimball D J, Yashchuk V and Budker D 2006 *Phys. Rev. A* **74** 063420
[5] Wang M L, Wang M B, Zhang G Y and Zhao K F 2016 *Chin. Phys. B* **25** 060701
[6] Xu C, Wang S, Feng Y, Zhao L and Wang L 2016 *Sci. Rep.* **6** 28169
[7] Huang H C, Dong H F, Hao H J and Hu X Y 2015 *Chin. Phys. Lett.* **32** 098503
[8] Graf M T, Kimball D F, Rochester S M, Kerner K, Wong C, Budker D, Alexandrov E B, Balabas M V and Yashchuk V V 2005 *Phys. Rev. A* **72** 023401
[9] Shah V, Vasilakis G and Romalis M V 2010 *Phys. Rev. Lett.* **104** 013601
[10] Grossetête F 1964 *Journal de Physique* **25** 383
[11] Bouchiat M and Brossel J 1966 *Phys. Rev.* **147** 41
[12] Happer W and Tang H 1973 *Phys. Rev. Lett.* **31** 273
[13] Allred J C, Lyman R N, Kornack T W and Romalis M V 2002 *Phys. Rev. Lett.* **89** 130801
[14] Appelt S, Ben-Amar Baranga A, Young A R and Happer W 1999 *Phys. Rev. A* **59** 2078
[15] Budker D, Kimball D F, Rochester S M, Yashchuk V V and Zolotorev M 2000 *Phys. Rev. A* **62** 043403
[16] Julsgaard B, Sherson J, Sørensen J L and Polzik E S 2004 *J. Opt. B: Quantum Semiclass. Opt.* **6** 5
[17] Chalupczak W, Josephs-Franks P, Pustelny S and Gawlik W 2010 *Phys. Rev. A* **81** 013422
[18] Chalupczak W, Godun R, Anielski P, Wojciechowski A, Pustelny S and Gawlik W 2012 *Phys. Rev. A* **85** 043402
[19] Gartman R and Chalupczak W 2015 *Phys. Rev. A* **91** 053419
[20] Auzinsh M, Budker D and Rochester S 2010 *Optically polarized atoms: understanding light-atom interactions* (Oxford: Oxford University Press) p. 198
[21] Grujić Z D and Weis A 2013 *Phys. Rev. A* **88** 012508
[22] Budker D and Kimball D F J 2013 *Optical magnetometry* (Cambridge: Cambridge University Press) pp. 280–306
[23] Qiu Y, Li H, Zhang S L, Wang Y L, Kong X Y, Zhang C X, Zhang Y S, Xu X F, Yang K and Xie X M 2015 *Chin. Phys. B* **24** 078501